Research Article Vol. 57, No. 34 / 1 December 2018 / Applied Optics F37

applied optics

Rapid fabrication strategy for ∅1.5 m off-axis parabolic parts using computer-controlled optical surfacing

Haixiang Hu,[1,*] Erhui Qi,[1] Xiao Luo,[1] Xuejun Zhang,[1,2] and Donglin Xue[1,2]

[1]Key Laboratory of Optical System Advanced Manufacturing Technology, Changchun Institute of Optics, Fine Mechanics and Physics, Chinese Academy of Sciences, Changchun, Jilin 130033, China
[2]University of Chinese Academy of Sciences, Beijing 100049, China
*Corresponding author: hhx@ciomp.ac.cn

Received 3 July 2018; revised 30 August 2018; accepted 30 August 2018; posted 31 August 2018 (Doc. ID 336256); published 24 September 2018

Off-axis parabolic parts (OAPs) or quasi-OAPs are mostly frequently used in large optical telescopes. Compared to the stressed mirror polishing, computer-controlled optical surfacing (CCOS) or other computer-controlled subaperture tools provide more flexibility. However, the fabrication efficiency needs to be promoted in tactical ways. In this paper, we present a large aperture CCOS lap equipped with a compound motion unit and go through the grinding and pre-polishing with its figure errors. A CCOS-based heterocercal tool is first used in large optics to restrain the edge effects. In the fine polishing stage, corrective polishing, smoothing, and ion beam figuring are applied in combination to finish. We experimentally test this strategy on an ∅1.5 m OAP, as a part of giant steerable science mirror (GSSM) in the Thirty Meter Telescope. Finally, the surface error of ∅1.5 m OAP is better than 1/50λ RMS (full aperture), and the mid-spatial frequency part is better than 0.64 μrad in slope RMS (effective aperture). The effective fabrication duration is reduced to 2 months.

https://doi.org/10.1364/AO.57.000F37

1. INTRODUCTION

An off-axis parabolic surface (OAP) is one type of all off-axis aspheres. Its conic constant κ is exactly −1. At the very first, OAP can be found in a Newton telescope. Nowadays, people still use OAP or quasi-OAP (means the conic constant is very close to −1) as the primary mirror in most telescope designs. OAPs or quasi-OAPs in the ∅1.5 m class are not that large but are the most frequently used. In nearly half of ultra-large optical telescopes (> ∅8 m), such as Gran Telescopio Canarias (GTC), Keck I & II, the primary mirror was built as a whole of ∅1.5 m class quasi-OAP segmented mirrors. The concept and necessary technologies were initially developed under the leadership of Dr. Jerry Nelson at the Lawrence Berkeley National Laboratory and University of California during the 1980s and have since spread worldwide to the point that essentially all future large optical telescopes plan to use segmented mirrors [1].

In the world-famous James Webb space telescope (JWST), Thirty Meter Telescope (TMT), and extremely large telescope (ELT) programs, more than 1500 pieces of ∅1.5 m quasi-OAPs (including spares) were planned to be finished within a decade. In 2017, China also considered joining the ranks of leading a giant telescope project. A proposal of a ∅12 m large optical/infrared telescope (LOT) was discussed [2], with its primary mirror possibly being made of 84 pieces of ∅1.5 m quasi-OAPs [3]. Thus, it is important to figure out a rapid fabrication strategy for the numerous segmented mirrors.

In 1980, Nelson developed the stressed mirror polishing (SMP) method for large off-axis OAP polishing [4]. SMP is the technique of applying specific loads to a part to warp out the nonspherical components of surface shape and then grinding and polishing the part spherically [5]. Spherical processing is much faster than alternative aspheric (small tool) processes, because much larger tools are used and the entire surface is worked at once. However, similarly to stressed lap polishing (SLP), it needs complicated facilities and precise calculation to build a set of devices [6]. To avoid concentration of stress, SMP can handle only shell mirrors [7] and certain material, so support and fixture are required to be extremely precise [5]. Thus, it is too time-consuming.

Computer-controlled optical surfacing (CCOS) processes have been developed and used in aspheric optics processing since 1963 [6–11]. In a CCOS process, the numeric-controlled machine drives a subaperture tool to go through the mirror surface, making a certain material removal at each place. The amount of the removed material is determined by the tool influence function (TIF) and the dwell time.

Based on the subaperture removing process, the CCOS method is applicable for almost all the fabrication conditions.

Table 1. Comparison of SMP and CCOS in ∅1.5 m OAP Fabrication

Category	SMP	CCOS
Material removal rate	✓ Fast material removal	Subaperture tool, slower
Surface quality—edge	✓ Better edge (generally)	Suffers from edge problems
Surface quality—MSE	✓ Few frequency error issues	Suffers from mid-frequency errors
Core devices	Complicated facilities and calculation	✓ Simple, versatile machine and tool
Material type	Zerodur shell	✓ Suitable for any optical material
Light-weighted parts	Cannot deal with structured parts	✓ Applicable for structured parts
Fixture and support	Thin mirror, high precision	✓ Can be solid part, lower requirement

However, the CCOS technique is still strongly limited by the low material removing rate, the edge effect, and the mid-spatial frequency errors (MSEs) [12–18]. Table 1 shows the advantages and disadvantages of SMP and conventional CCOS in large OAP fabrication.

We are working on a ∅1.5 m interferometer for the tertiary mirror (M3) of the TMT project in Changchun Institute of Optics, Fine Mechanics and Physics (CIOMP). M3 is an elliptical flat mirror, 3.5 m × 2.5 m across [19]. Thus a ∅1.5 m OAP illuminating mirror has been planned to test the world's largest optical flat as part of the Giant Steerable Science Mirror (GSSM) system. The optical testing layout is shown in Fig. 1.

As to a single mirror, if we produce a set of SMP facilities, the cost and period are unacceptable. In this paper, a so-called rapid fabrication strategy using the CCOS method is presented for the ∅1.5 m OAP processing. Focused on the efficiency issues in conventional CCOS, here we mainly present three key technologies to deal with the tool-size limitation, edge effects, and MSE problems.

In Section 2, some basic information of ∅1.5 m OAP will be given at first, along with a brief description of the support system and testing method. In Section 3, a heterocercal sandwich tool will be introduced to deal with the edge effect for large tools. In Section 4, bandpass slope RMS is used as smoothing indicator. Smoothing-after-figuring process is put into use to avoid surface error relapse and reduce iteration loops.

At the end of each section, the experimental records will be shown, analyzed, and discussed. As a summary, the whole processing period chart will be presented in the last section, which shows that by means of our rapid fabrication strategy, the ∅1.5 m OAP can be finished in 2 months.

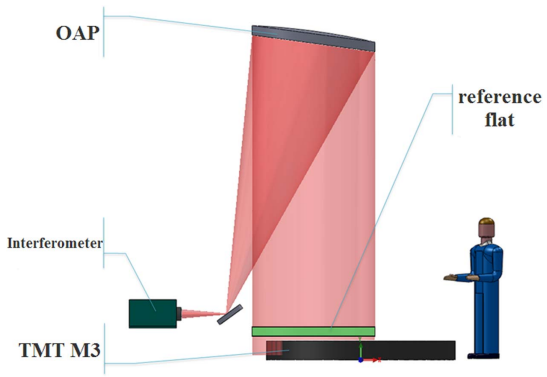

Fig. 1. M3 mirror optical testing with OAP illumination layout.

2. EFFICIENT FABRICATION STRATEGY USING CCOS METHOD

The ∅1.5 m OAP mirror is made of Corning ULE, and some essential information is given in Table 2.

A. Testing Condition

In the grinding stage, we tested the surface error via swing arm profilometer within ~1/10λ RMS accuracy [20]. As shown in Fig. 2, the *in situ* swing arm can compress the period of a processing iteration to grind and test.

While in the polishing stage, surface errors can be obtained by interferometry testing using a null lens as the compensator. The horizontal optical layout is the primary testing status for the entire polishing stage, as shown in Fig. 3. After finishing, the mirror will be tested in the facedown status, which is the final state.

B. Fast Support

To ease the support structure, a simple three-point support is presented for fabrication [21]. The CCOS method can live

Table 2. Essential Parameter of the ∅1.5 m OAP

Boundary Dimension		Material Parameters	
Item	Value	Item	Value
ROC	10 m	Density	2.21 g/cm^3
∅	1.431 m	E	67.6 Gpa
Max. thickness	160 mm	Poisson ratio	0.17
Off-axis	1.0 m	MOR	49.8 Mpa

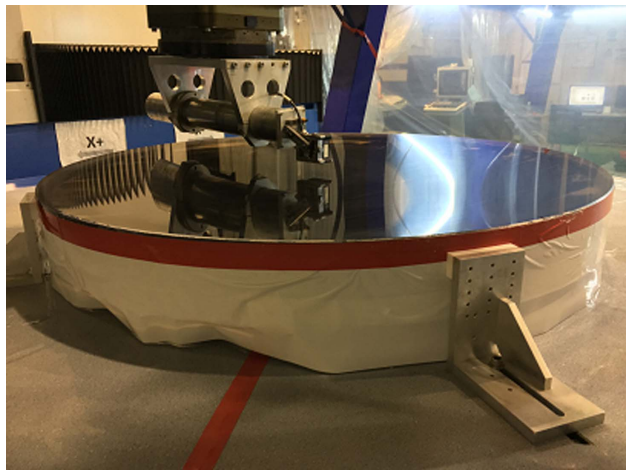

Fig. 2. ∅1.5 m OAP *in situ* testing using swing arm profilometer.

Fig. 3. ∅1.5 m OAP optical testing layout.

through the low-order print-through surface error induced by gravity deformation [22], but the testing cannot. The distance between the support points is much bigger than the tool size, so the print-through effect will not leave obvious MSEs. However, the deformation affects testing results directly. Hence, a digital pattern was used to correct the deformation error, after a self-calibration process.

The simple support structure is to be designed as three independent ball and socket joints and then covered with a Teflon protection layer, as shown in Fig. 4. As to the finite elements analysis (FEA) model, the boundary condition is clear enough to get a convinced deformation result. The three supporting points are uniformly distributed, 500 mm from the center of mirror. The contact area is ∅150 mm for each point. The FEA model divides 57,757 units (~30 mm spacing) and 85,748 nodes. Here, gravity acceleration $g = 9.81$ N/m2.

As shown in Fig. 4, the self-weight deformation is PV1.15 μm, RMS0.278 μm, and the main aberration is trefoil. Subtract that from the swing arm testing results, and we will get the actual surface errors.

To decouple the fabrication residual errors and deformation errors in actual surface testing, a self-calibration method is illustrated. The mirror under test is kept still, while the support points are rotated 180°. Through the FEA model, the change of surface error can be obtained. At the same time, the same operation can be done in actual mirror testing. Comparing the two difference maps, as shown in Fig. 5, the Zernike coefficient can be fitted to refine the nominal elasticity modulus.

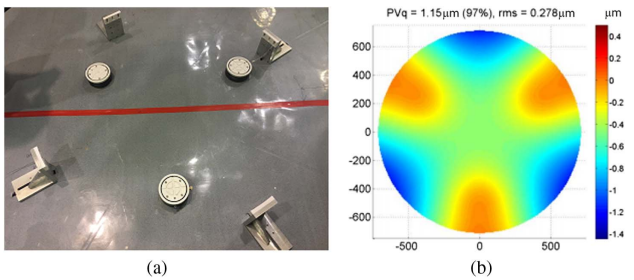

Fig. 4. Gravity deformation on three-point support by FEA. (a) Location of three supporting points. (b) Self-weight deformation map.

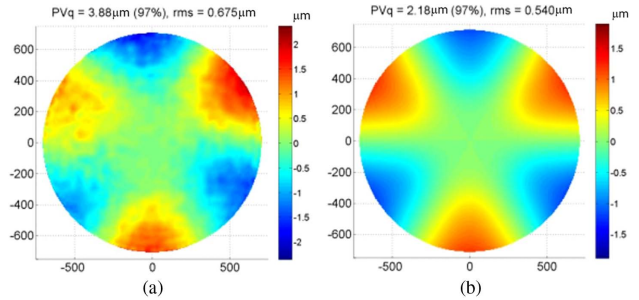

Fig. 5. Difference map as supporting points rotate 180°. (a) Profilometer testing result. (b) FEA result.

In the FEA model, the coefficient of trefoil error (in fringe Zernike terms) is PV 2.97 μm, while in the swing arm result, PV = 3.56 μm. The digital pattern is prepared as the FEA results of gravity deformation enlarge by 19.5%. A self-calibrated digital pattern is put into use in profilometer testing throughout the grinding process. Thus, the fabrication and testing accuracy would be affected within the limitation of the profilometer instead of supporting precision.

C. Rapid Grinding and Polishing Strategy

With a sufficient testing and supporting condition, we plan our rapid fabrication strategy in both grinding and polishing stage.

Stage 1 uses a large semi-rigid heterocercal tool in the grinding stage. The mismatch between the rigid tool and the aspheric surface limits the selection of tool size, meaning a low material removal efficiency. Furthermore, half-rigid tools suffer extremely from the edge effect problem. We combine the sandwich tool and heterocercal tool to make it more suitable for large aspheric optics edge polishing.

Stage 2 uses a two-tool combination in the fine polishing stage. A kind of smoothing-after-figuring iteration, especially for large tools and small tools, is presented. Using bandpass slope RMS as the index, the smoothing process is judged to be continuous and stable. Finally, by means of ion beam figuring (IBF), the mirror will be finished with both high efficiency and accuracy.

3. RAPID GRINDING STRATEGY

In the grinding stage, a large amount of material removal should be achieved to ensure the minimal residual of subsurface damage. The conventional CCOS method suffers from a lack of efficiency due to a mismatch and the edge effect [23,24]. In this part, we demonstrate the grinding process using the semi-rigid sandwich tool and the edge-controlled heterocercal tool to break through the tool size limitation.

A. Edge Effect Issues

Edge effect matters directly because of the tool's overhang. Less overhang leaves the edge of the mirror rolling up. More overhang is worse. It makes edge rolling down much different from what was expected [23]. Here we give some models to describe this situation. While in OAP processing, the mismatch compounds the edge effect, and makes it more difficult to predict

and more significant. Hence the tool overhang needs to be controlled for a better edge.

We provided the idea of a skewed TIF to deal with the problem [25]. We call it the heterocercal tool, because the skewed shape was inspired by the heterocercal tail of sharks. The concept of a heterocercal tool is to combine continuous orbital motion with swing rotation. When the tool moves near the edge, the resultant velocity between the tool and the mirror is enlarged at the edge and is reduced inside. As a result, material removal is transferred toward the edge, leaving less turned-up edge residual. It will be good for the edge material removal. On the other hand, equipped with a heterocercal motion unit, tool size can be larger.

B. Aspheric Mismatch

The application of large tools is difficult in an asphere. Because the local curvature of the surface varies here and there, the tool will not match the work piece when travelling throughout the mirror, leaving a significant gap in between, as follows:

$$\delta \approx \frac{D^2}{8}\Delta k. \tag{1}$$

Here, δ stands for the mismatch gap, D for tool diameter, and Δk for the difference in curvature. Generally, it is rigid tool intrinsic issues. The changing local curvature makes the tool mismatch. From Eq. (1), we can see that the curvature mismatch will increase rapidly, if the tool is getting large in diameter. In the early process of ∅1.5 m OAP, the tool we used is a ∅200 mm cast iron; then we get strong waviness round the mirror, as shown in Fig. 6. That means the size is limited using rigid tools, even though heterocercal motion unit is equipped.

We tried a semi-rigid tool type, a so-called sandwich tool. It combines a rigid thin plate and flexible foam between the grolishing media and tool body. The plate can still provide the stiffness in mid-spatial frequency when bending to fit the mirror. The load inhomogeneity brought in by that should be calculated and designed with Eq. (2), as follows:

$$\Delta\Delta w(x,y) = \frac{1}{D}\cdot q(x,y), \qquad \text{with } D = \frac{Eh^3}{12(1-\nu)}. \tag{2}$$

The bending of tool plate is varied in a different subaperture of the aspheric surface. With the help of Eq. (2), the load inhomogeneity can be obtained by the change of bending. On the other hand, parameters like the plate thickness can be designed with the load inhomogeneity allocation.

The foam is to create a nearly equal press in a different extent of strain. A schematic 3D model for a semi-rigid sandwich lap is depicted in Fig. 7. It is a grolishing tool filled with foam in between. The foam is contained between the tool base and thin plate.

We did the combination and made a ∅300 mm heterocercal sandwich tool. The load inhomogeneity was controlled under 5%.

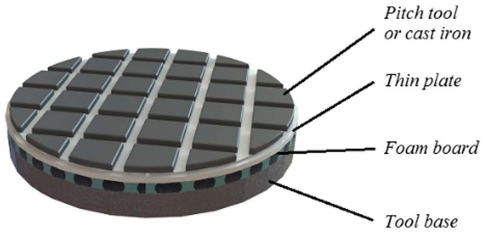

Fig. 7. Semi-rigid tool type with the sandwich structure.

C. Actual Processing Instance

In this part, the ∅300 mm heterocercal sandwich tool (made of 28 pieces of ∅40 mm cast iron) is applied in ∅1.5 m OAP grinding, as shown in Fig. 8, using W14 SiC abrasive grits. The stroke radius of orbital motion is 20 mm, minimum pin-to-edge distance is 120 mm, and the pressure is 1.95 kPa. Heterocercal coefficient is optimized to be 0.18. Simulation software for the large aspheric mirror (SLAM, developed by CIOMP) is used to calculate the dwell time, in which the calculation is based on the matrix algorithm [26]. Total processing time is about 40 min (7000 revolutions at 200 rpm spindle speed).

Figure 9(a) shows the initial surface error map is 0.25 μm in RMS. Figure 9(b) shows the residual error map after grinding, which is 0.18 μm in RMS. Figures 9(c) and 9(d) show the material removal distribution in simulation and in the actual process. The aimed and actual convergence rates of RMS were 36% and 28%, respectively. We can see quite a good consistency and precision in material removal. And more important, the mirror does not suffer from mismatch waviness, looking more like an axial piece than an off-axis one. We used the

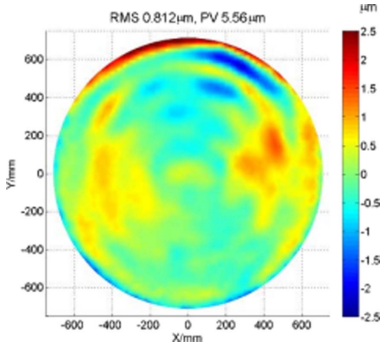

Fig. 6. Rigid tool intrinsic ringing effects when grinding ∅1.5 m OAP.

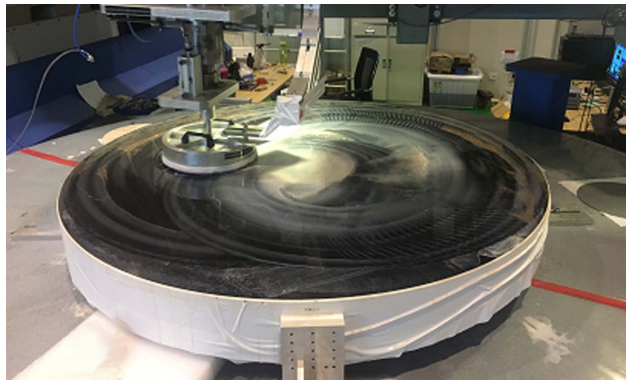

Fig. 8. ∅300 mm heterocercal sandwich tool on ∅1.5 m OAP.

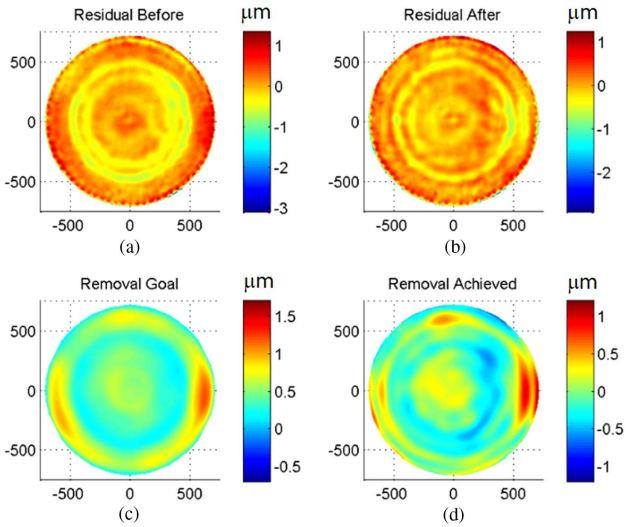

Fig. 9. Run of large heterocercal sandwich tool grinding. (a) Surface errors before fabrication. (b) Surface errors after fabrication. (c) Aimed material removal distribution. (d) Actual material removal distribution.

Ø300 tool from grinding through polishing. It helped us to speed up the processing period.

After grinding and prepolishing, the surface error can be tested by an interferometer with a horizontal optical layout. In the horizontal testing state, the self-weight deformation is not larger than 6 nm RMS (estimated by FEA). The optical testing result (first light) shows PV 2.1λ, RMS 0.22λ($\lambda = 0.6328$ μm), as shown in Fig. 10. There is no obvious trefoil aberration, or print-through effect; thus, the fast support device and digital pattern calibration presented above are effective.

There is a lot of nonavailable area due to the roughness of the surface, and the mid-to-high frequency errors appear due to the nonuniform sub-surface damage layer induced by subaperture tools. Once polished out, the surface would be better.

The total grinding process includes 25 loops of grinding-testing iteration and takes 34 days.

4. RAPID SMOOTHING AND FIGURING STRATEGY

In the polishing stage, smoothing and figuring are usually used as a combination [27]. However, this stage relies heavily on experience to decide when to figure or to smooth. In this part, we tested a rapid smoothing and figuring strategy with the following three steps:

Step 1, after a sufficient prepolishing, make an iteration loop with a proportional figuring and smoothing, and then testing.
Step 2, continuously smooth the surface with a large tool and use bandpass slope RMS as the indicator.
Step 3, make the final figuring using IBF.

We decide the transition from Step 1 to Step 2, once the residual material removal volume is small enough for the IBF process. Otherwise the IBF process will take too much time. As to our case, Ø1.5 m, ULE material, the judgment is around 0.2λ in RMS.

The smoothing to the IBF transition point is determined by the high-passed surface error RMS. The σ of the high-passed Gaussian filter is same as the σ of the IBF spot. Once the high-passed RMS meets the requirement of RMS specification (of all frequency, not filtered), it is time for the IBF.

A. Smoothing-After-Figuring Loop

The smoothing–figuring loop is to make up a single processing iteration with figuring, smoothing, and testing sequentially, instead of figuring–testing–smoothing–testing. We utilized this strategy to shorten the iteration cycle and ensure the convergence rate of each processing loop. It is essential to decide the proportion of figuring and smoothing, and related working parameters, such as tool sizes, pressure, and spindle speed. Jones developed a general simulation model for CCOS smoothing in 1995 [28].

Through the simulation, we find that the best ratio of smoothing tool size to the MSE spatial cycle is larger than 3, hence the size of figuring TIF should be selected smaller than 1/3 of smoothing tool size. In the actual process, Ø300 mm smoothing tool and Ø50 mm figuring tool were put into use.

To ensure a considerable smoothing efficiency, we still used the semi-rigid sandwich tool with 40 mm pitch square uniformly pasted. The Ø50 mm figuring tool's interface with the workpiece was a covered LP-66 polyurethane (PU) pad on pitch. The stroke radius of figuring was 10 mm and made the TIF 70 mm in width, as shown in Fig. 11. The polishing abrasive is Unicer3 from Universal Photonics. The revolution speed for figuring is ~300 RPM.

The proportion of smoothing and figuring is calculated by balancing the convergence rate and smoothing coefficient. Table 3 presents the entire process of the smoothing-after-figuring loop. The average convergence rate of RMS is 22.6%.

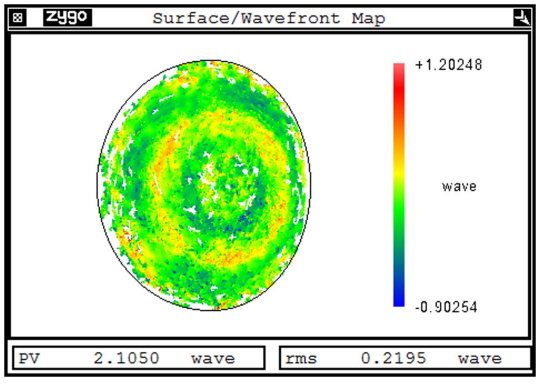

Fig. 10. First optical testing result of Ø1.5 m OAP.

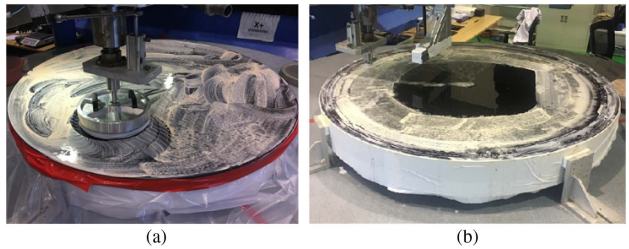

Fig. 11. Ø1.5 m OAP smoothing-after-figuring process.

Table 3. Smoothing-After-Figuring Settings and Response in Each Loop

Loop#	Figuring Revs	Smoothing Revs	PV/λ	RMS/λ	Band-Pass Slope RMS/μrad
#1	40 k	30 k	2.98	0.39	2.15
#2	100 k	60 k	2.72	0.34	1.82
#3	50 k	50 k	2.18	0.29	1.92
#4	110 k	15 k	2.12	0.24	1.88
#5	180 k	12 k	1.18	0.14	1.60

Table 4. Smoothing Settings and Response in Each Loop

Loop#	Duration/h	Smoothing Revs	PV/λ	RMS/λ	Band-Pass Slope RMS/μrad
#6	15	15 k	1.55	0.23	1.31
#7	12	12 k	1.47	0.23	1.24
#8	11	11 k	1.57	0.25	1.04

B. Continuously Smoothing

Different from the figuring, CCOS smoothing efficiency is not linearly relevant to spindle speed and pressure but more like a threshold effect. To check the velocity-irrelevant effect, we set the spindle speed down to ~20 rpm. The tool pressure for continuously smoothing is around 2 kpa, or 0.3 psi. The bandpass slope RMS was utilized to indicate the smoothing effect. Here, the filter high/low wavelength was set to 10 mm/50 mm, and the sampling grid size was 3.4 mm. Table 4 shows that after the entire three loops of smoothing, the MSE was reduced to 1.0 μrad in the bandpass slope RMS. The average convergence rate of that is 13.3%.

After that, the mirror was directly sent to IBF for final figuring. The working duration of IBF was 10 days. The surface error remains 0.019λ RMS in full aperture, as shown in Fig. 12. While in ∅1.33 m effective aperture the final surface error is 1/60λ in RMS and 0.64 μrad in slope RMS (not bandpassed).

C. Discussion

In the ∅1.5 m OAP polishing, we used a three-step strategy to achieve 1/50 ~ 1/60λ RMS surface accuracy. This convergence process is stable without obviously MSE relapse. As shown in Fig. 13, in the smoothing-after-figuring stage (Loop 1–5), low-order surface error and MSE converge consistently. While in the smoothing stage (Loop 6–8), the MSE converges at a similar rate, but the low-order surface error is enlarged. Even so, after IBF, the surface accuracy is still good in both RMS and slope RMS judgment.

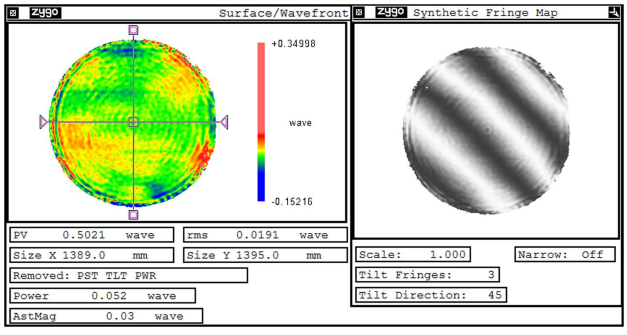

Fig. 12. ∅1.5 m OAP surface final residual map.

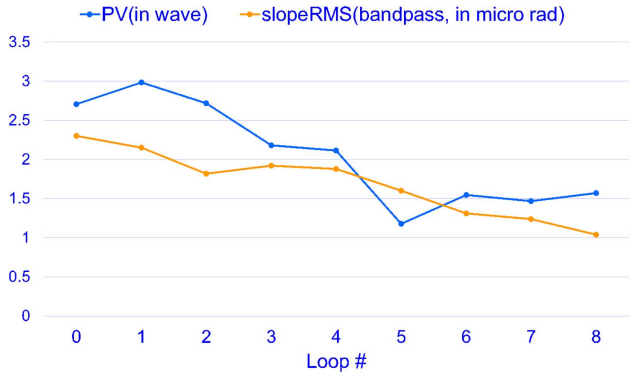

Fig. 13. ∅1.5 m OAP surface error tendency in CCOS polishing stage.

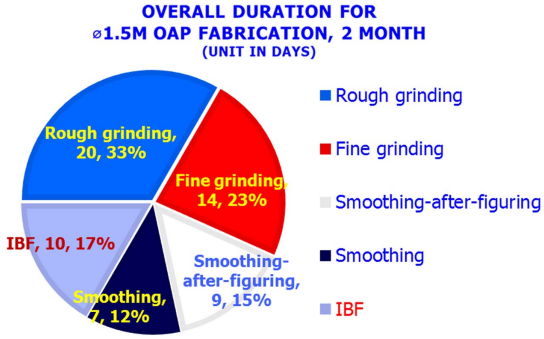

Fig. 14. ∅1.5 m OAP grinding and polishing duration (effective).

To summarize the rapid fabrication strategy, we make the statistical data of the entire fabrication duration. The total grinding and polishing process was 2 months, as shown in Fig. 14.

5. CONCLUSION

In this paper, rapid fabrication strategy for ∅1.5 m OAP is presented. We discussed the fabrication process of 1.5 m class OAP, including the fast support, semi-rigid sandwich tool, the edge-controlled heterocercal tool, and the smoothing

and figuring combination. The final surface errors are $\sim 1/60\lambda$ in RMS and 0.64 μrad in slope RMS, meeting the requirement to the illuminating mirror well. Taking account of the grinding and polishing period, the effective processing duration is about 2 months for ∅1.5 m OAP. The short fabrication period shows validity of the presented rapid fabrication strategy.

Still the grinding process takes too much working time. We believe there is lot of overgrinding work wasted. Future work is to perform the removal property of subsurface damage with different grinding parameters for more efficient fabrication in the low precision stage.

Funding. National Natural Science Foundation of China (NSFC) (61210015); Key Research Program of Frontier Sciences, Chinese Academy of Sciences (CAS) (QYZDJ-SSW-JSC038-02).

Acknowledgment. The authors, especially Haixiang Hu and Erhui Qi would like to thank the technical communication with Glen Cole, whose advice is extremely helpful in actual processing.

REFERENCES

1. https://en.wikipedia.org/wiki/Segmented_mirror.
2. X. Cui, Y. Zhu, M. Liang, D. Su, X. Yuan, Z. Hu, H. Bai, and B. Gu, "Introduction on Chinese 12 m optical/infrared telescope (LOT)," Proc. SPIE **10700**, 107001P (2018).
3. D. Ma, "Recommended conceptual optical system design for China's large optical-infrared telescope (LOT)," Opt. Express **26**, 108–119 (2018).
4. J. E. Nelson, G. Gabor, L. K. Hunt, J. Lubliner, and T. S. Mast, "Stressed mirror polishing. 2: fabrication of an off-axis section of a paraboloid," Appl. Opt. **19**, 2341–2352 (1980).
5. L. M. Stepp and S. F. Sporer, "TMT: stressed mirror polishing fixture study," Proc. SPIE **6267**, 62672R (2006).
6. L. M. Stepp, D. S. Anderson, H. M. Martin, J. H. Burge, D. A. Ketelsen, and S. C. West, "Rapid fabrication strategies for primary and secondary mirrors at Steward Observatory Mirror Laboratory," Proc. SPIE **2199**, 199–210 (1994).
7. A. E. Hatheway, J. S. Johnson, K. D. Grobsky, and D. Bray, "Rapid fabrication of lightweight silicon-carbide mirrors," Proc. SPIE **4771**, 243–253 (2002).
8. V. Rupp, "The development of optical surfaces during the grinding process," Appl. Opt. **4**, 743–748 (1965).
9. R. A. Jones, "Optimization of computer controlled polishing," Appl. Opt. **16**, 218–222 (1977).
10. R. A. Jones, "Computer-controlled optical surfacing with orbital tool motion," Opt. Eng. **25**, 256785 (1986).
11. J. Zimmerman, "Computer controlled optical surfacing for off-axis aspheric mirrors," Proc. SPIE **1236**, 663–668 (1990).
12. N. Yaitskova and M. Troy, "Rolled edges and phasing of segmented telescopes," Appl. Opt. **50**, 542–553 (2011).
13. D. D. Walker, G. Yu, H. Li, W. Messelink, R. Evans, and A. Beaucamp, "Edges in CNC polishing: from mirror-segments towards semiconductors, paper 1: edges on processing the global surface," Opt. Express **20**, 19787–19798 (2012).
14. H. Li, D. Walker, G. Yu, A. Sayle, W. Messelink, R. Evans, and A. Beaucamp, "Edge control in CNC polishing, paper 2: simulation and validation of tool influence functions on edges," Opt. Express **21**, 370–381 (2013).
15. H. Liu, F. Wu, Z. Zeng, B. Fan, and Y. Wan, "Edge effect modeling and experiments on active lap processing," Opt. Express **22**, 10761–10774 (2014).
16. E. Luna-Aguilar, A. Cordero-Davila, and J. Gonzalez, "Edge effects with Preston equation," Proc. SPIE **4840**, 598–603 (2003).
17. A. Cordero-Davila, J. González-Garcıa, M. Pedrayes-Lopez, L. A. Aguilar-Chiu, J. Cuautle-Cortes, and C. Robledo-Sanchez, "Edge effects with the Preston equation for a circular tool and workpiece," Appl. Opt. **43**, 1250–1254 (2004).
18. H. S. Nam, G. C. Kim, H. S. Kim, H. G. Rhee, and Y. S. Ghim, "Modeling of edge tool influence functions for computer controlled optical surfacing process," Int. J. Adv. Manuf. Technol. **83**, 911–917 (2016).
19. V. G. Ford, Thirty Meter Telescope Observatory Corporation document, "Tertiary mirror surface figure specification," (2014).
20. L. Xiong, X. Luo, H. Hu, Z. Zhang, F. Zhang, L. Zheng, and X. Zhang, "Swing arm profilometer: high accuracy testing for large reaction-bonded silicon carbide optics with a capacitive probe," Opt. Eng. **56**, 084101 (2017).
21. A. Ahmad, "Low-cost adjustable mirror mount," Opt. Eng. **33**, 2062–2064 (1994).
22. H. Hu, X. Luo, and H. Xin, "Layout optimization of equal-force supports for ultra large optical fabrication," Acta Opt. Sin. **34**, 0422003 (2014).
23. D. W. Kim, W. H. Park, S. W. Kim, and J. H. Burge, "Parametric modeling of edge effects for polishing tool influence functions," Opt. Express **17**, 5656–5665 (2009).
24. R. Rascher, O. Fähnle, C. Wünsche, C. Schopf, and W. A. C. M. Messelink, "Aspheric mismatch of rigid tools," Proc. SPIE **10009**, 1000904 (2016).
25. H. Hu, X. Zhang, V. Ford, X. Luo, E. Qi, X. Zeng, and X. Zhang, "Edge control in a computer controlled optical surfacing process using a heterocercal tool influence function," Opt. Express **24**, 26809–26824 (2016).
26. L. Li, L. Zheng, W. Deng, X. Wang, X. Wang, B. Zhang, Y. Bai, H. Hu, and X. Zhang, "Optimized dwell time algorithm in magnetorheological finishing," Int. J. Adv. Manuf. Technol. **81**, 833–841 (2015).
27. J. L. Bentley, D. W. Kim, H. M. Martin, J. H. Burge, and M. Pfaff, "Optical surfacing process optimization using parametric smoothing model for mid-to-high spatial frequency error control," Proc. SPIE **8884**, 88840B (2013).
28. R. A. Jones, "Computer simulation of smoothing during computer-controlled optical polishing," Appl. Opt. **34**, 1162–1169 (1995).